
Article:
Yeo, S., Komatsu, K., Hsu, M.-F. et al. (2 more authors) (2018) Structural behavior of traditional Dieh-Dou timber main frame. International Journal of Architectural Heritage: conservation, analysis, and restoration. ISSN 1558-3058

https://doi.org/10.1080/15583058.2018.1442518

Structural behaviour of traditional Dieh-Dou timber main frame

Sok-Yee Yeo*[a], Kohei Komatsu[a,1], Min-Fu Hsu[a], Yu-Lin Chung[a], Wen-Shao Chang[b]

[a] Department of Architecture, National Cheng Kung University,
No. 1 University Road, Tainan city, 70101, Taiwan R.O.C
[b] Sheffield School of Architecture, The University of Sheffield,
Art Tower, Sheffield, S10 2TN, United Kingdom

***Corresponding author** Tel: +886-62757575 ext. 54151; Fax: +886-62083973; Email address: yanzyeo@gmail.com

Abstract (250 words)

Under different combinations of horizontal and vertical loads, a total of three static cyclic tests were conducted to investigate the in-plane structural behaviour of the traditional Dieh-Dou timber frame. Typical deformation patterns include column rocking, joint rotation around the primary beam-column and column Dou-column regions, vertical shear around the upper and lower end of column mortise, embedment around primary beam-column regions and vertical shearing around the mortise regions of the Dou members. Visible deformation generally began from 1/30 rad onwards. Column restoring force contributed mainly to the main frame's moment resistance when displacement is small. When frame deformation exceeds 1/50 rad, bending moment from the primary beam dominated the frame's global restoring force. Hence, column restoring force and the primary beam-column connection generally undertake the primary moment-resisting mechanism while the complex bracket structures above the primary beam play a secondary role. Base on embedment theory and semi-rigid spring model, a new theoretical model was developed to estimate the global behaviour for the global system of Dieh-Dou main frame. The current model can only estimate the initial and secondary stiffness as the spring stiffness are assumed to behave bi-linearly. Hence, it is unable to predict the out-of-plane failure phenomena and ultimate failure load at this moment. Although the prediction tends to be on the conservative side, the predicted model is generally in good agreement with observed results.

Keywords:
Static test, traditional timber frame, beam-column joint, rotational stiffness, semi-rigid, embedment

[1] Present affiliation and address: Professor Emeritus of Kyoto University, Research Institute for Sustainable Humanosphere (RISH), Gokasyo, Uji, Kyoto 611-0011, Japan. Tel.: (+81) 774-38-3679.

1. INTRODUCTION

Dieh-Dou timber frame, commonly found in Taiwan, southern China, Singapore and Malaysia, is traditionally used in the construction of temples, ancestral halls and residential houses of rich people. The layout plan of a typical Dieh-Dou timber building consists of three to five Jian (bays), subjected to the owner's design requirement and budget (Figure 1). The building width of the Ming Jian (central bay) is usually wider than the two Ci Jian (side bays) as the central bay is commonly used for ceremonial and/or important functions.

Due to its spatial importance, a pair of Dieh-Dou 'Jia-Dong' timber frames is designed within the central bay region (Figure 1). For simplicity, this pair of timber frame will be referred as the 'Jia-Dong' frames. The Jia-Dong frames are further connected with another pair of horizontal tie members and Dou-Gong members that runs along the building width direction ('Pai-Lou' frames) to form a semi-rigid enclosed rectangular timber frame system. In this paper, main focus will be targeted on the structural behaviour of the Jia-Dong upper frame within the central bay region.

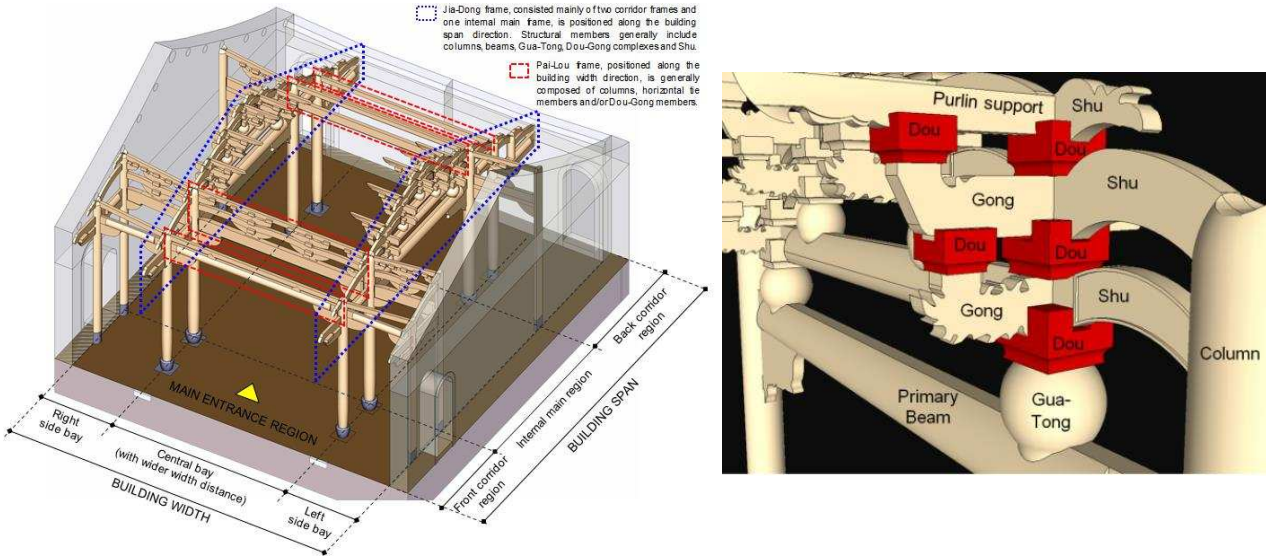

Figure 1. A typical Taiwanese Dieh-Dou timber building layout design [1] and naming of key structural members.

As shown in Figure 1, one complete set of Jia-Dong timber frame is composed of two corridor frames and one internal main frame. Starting from the Gua-Tong members (short vertical post-like members) that sit on top of the primary beam, the 'Dieh-Dou complex' can be viewed simply as a series of Dou-Gong brackets stacked one on top of the other, and further held together by a series of horizontal tie members (Shu members and secondary and/or tertiary beams) to form a triangular mass of timber upper structures. Regardless of the complexities of the upper structures, the heavy roof loads will eventually transmit down to the ground via these multiple-tier complex bracket structures, the Gua-Tong members, the Shu members, and finally to the structural resisting primary beam-column components.

In 1999, many invaluable Taiwanese historic timber structures were destroyed or seriously damaged during the Chi-Chi earthquake. Since then, a series of research was initiated to investigate the seismic performance of the Taiwanese traditional timber structures. From the post-earthquake reconnaissance literature [2-7], three main types of fracture modes were commonly observed in the Dieh-Dou timber frame buildings, namely, joint dislocation at both the timber column–beam region and timber column base–stone column/plinth connections that subsequently led to a partial collapse of the global frame (Figure 2a and 2b); vertical shear failure at the timber column–beam region (Figure 2c); and lastly, vertical and horizontal shear crack of adjoining members of the complex bracket system (Figure 2). More than a decade has passed since the Chi-Chi earthquake, but relatively few fundamental studies on the structural behaviour of Dieh-Dou timber frames and its joint connections [8-16] can be found to-date. Thus, there is an urgency to evaluate the seismic performance of the existing Dieh-Dou timber frame buildings so as to better protect the remaining Dieh-Dou type historic buildings from future earthquake attacks.

Majority of the research relating to the mechanical behaviour of Dieh-Dou timber frame arise from Japan [17-26], followed by Taiwan [8-16] and China [27-30]. Even though the Japanese traditional timber structures generally differs from the Taiwanese Dieh-Dou type, both traditional timber frames share key features such as the heavy roof loads, the common stacking characteristics of the Dou-Gong complex brackets and the beam-column penetrating joint concept. Furthermore, the traditional timber frames from both regions reside within the same seismic belt; hence, due to its close relevancy to the Taiwanese context, decision was made to employ the Japanese structural analytical approach.

Base on the studies conducted by Ban [17,18] and Suzuki [24,25], the structural mechanism of traditional timber frame structures has been established. The importance of column restoring force and beam-column connections play a crucial role towards the stability of the global structure. When the frame deformation is small, most of the moment-resisting responsibility falls on the column restoring force. But when the deformation angle gets larger, bending moments from the tie beams tends to take over most of the moment-resistance role. The ability of traditional timber structure to withstand large flexibility and deformability is commonly observed in the oriental traditional timber structures [24,25].

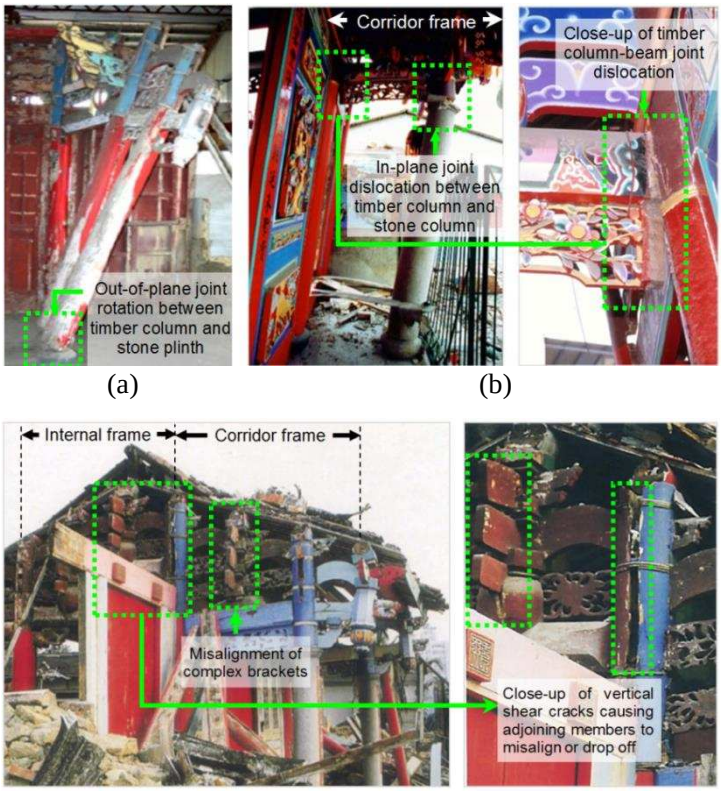

Figure 2. Typical damages observed in Dieh-Dou timber frame after the Chi-Chi earthquake: Joint dislocation occurring at (a) timber column base–stone column [7] and (b) timber column–beam region [6] and, (c) Shear crack causing misalignment of complex brackets [6]

By applying semi-rigid connections, in the form of rotational springs, during structural analysis of these traditional structures, it not only addresses the phenomenon of changing moment distribution among beams and column, but also helps to account for the increase of frame deflection and the subsequent increase of the force-displacement effect in the frame analysis [8,27,28]. Hence, it is more logical to consider the joint connections of the oriental timber structures as semi-rigid so that the predicted outcomes will be much closer to the actual behaviour. The performance of the traditional timber structure will only work best when it is subjected to a heavy roof load as the mortise-tenon and dowel connections can be tightly held in place and eventually, helps to contribute to a stiffer global frame to resist lateral force attack [8,13,14-16,27,28]. Since embedment of timber members is a natural outcome, it is therefore recommended to consider the triangular and complete embedment concepts proposed by Inayama [19-20] and Kitamori [26], respectively, during the mechanical modelling.

From the above studies, it is clear that the structural performance of traditional oriental timber structures relies on the rotational stiffness of the semi-rigid joints under the presence of heavy dead load. The seismic behaviour of the Taiwanese Dieh-Dou corridor upper structures has been studied [15,16], but the structural behaviour of its internal main frame's upper structures have yet been fully understood [8,14]. Thus, the main goal in this paper is to assess and compare the global behaviour of the upper structures of the internal main frame when subjected to different combinations of vertical and horizontal loads and beam-column joint designs. A series of static cyclic tests was applied to three specimens until large deformation. As the Japanese analytical approach will be used to work out the mechanical models of the test specimens, general concepts on the implementation of the Japanese approach onto the basic behaviour of the Dieh-Dou structure elements will be explained in section 3. The derived models were then verified with the experiment data to evaluate the validity of the theoretical assumptions made.

2. STATIC LATERAL CYCLIC TEST OF THE DIEH-DOU TIMBER FRAMES

The prototype design of the specimen mainly originates from an existing traditional Dieh-Dou timber frame that was once part of the Entrance Hall of the Chung Family Ancestral Hall at Ping-tung County in southern Taiwan (Figure 5a). Generally, the geometric dimensions of individual members of the test specimens are based on the initial design of the Entrance Hall corridor frame section. A total of three static tests focusing on the Dieh-Dou internal main frame were carried out. The test parameters mainly include different combinations of vertical and horizontal loads and joint design types for the primary beam-column connections.

2.1. Design of test specimens

2.1.1. Choice of frame design

As shown in Figure 3a, the prototype design of the upper structures of the internal main frame was supported by a half timber column cladded brick wall (left) and one timber composite column (right). Other commonly seen designs for the Dieh-Dou internal frame include the 'two beams-three Gua-tong' type and the 'three beams-five Gua-tong' type (Figure 3b), both of which are usually supported by two columns. As there is no strict rule governing the choice of Dieh-Dou timber frame design; hence, frame design selection is more often subjected by the availability of land and the builders' aesthetic preferences and financial resources. Due to the limitation of the reaction test frames, the design of the specimen was simplified to 'two beams-three Gua-tong' type (Figure 4), where the geometric dimensions of most of the structural members (except the column height and primary beam) were followed as closely to the initial design of the Entrance hall as possible (Figure 3a, box-up region).

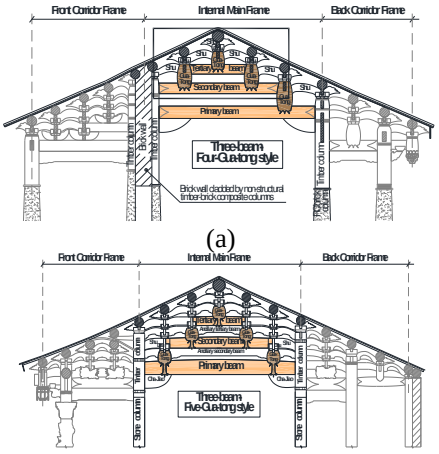

(a)

(b)

Figure 3. Variations of Dieh-Dou internal frame design: (a) 'three beams-four Gua-tong' type (Prototype's design) and (b) 'three beams-five Gua-tong' [31]

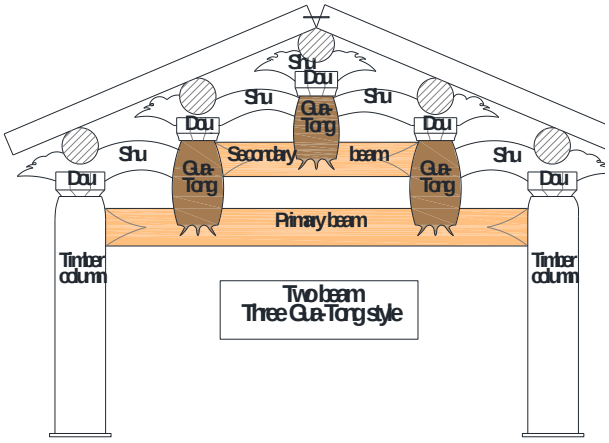

Figure 4. Final design of the test specimen: 'Two beams-three Gua-tong' composition

2.1.2. Choice of joint type design

Base on the traditional Taiwanese Master carpenters' practice, the choice of joint design for the primary beam-column depends on the overall self-weight of the timber frame of a particular section, without taking account on the roofing materials weight from purlin onwards. Thus, the Master carpenters will consider the front and back corridor frames to be comparatively 'lighter' than the 'heavier' internal main frame. As a result, the joint of primary beam-column for the corridor frame and internal frame will usually be designed as half-lap joint and butt joint, respectively (Figure 5).

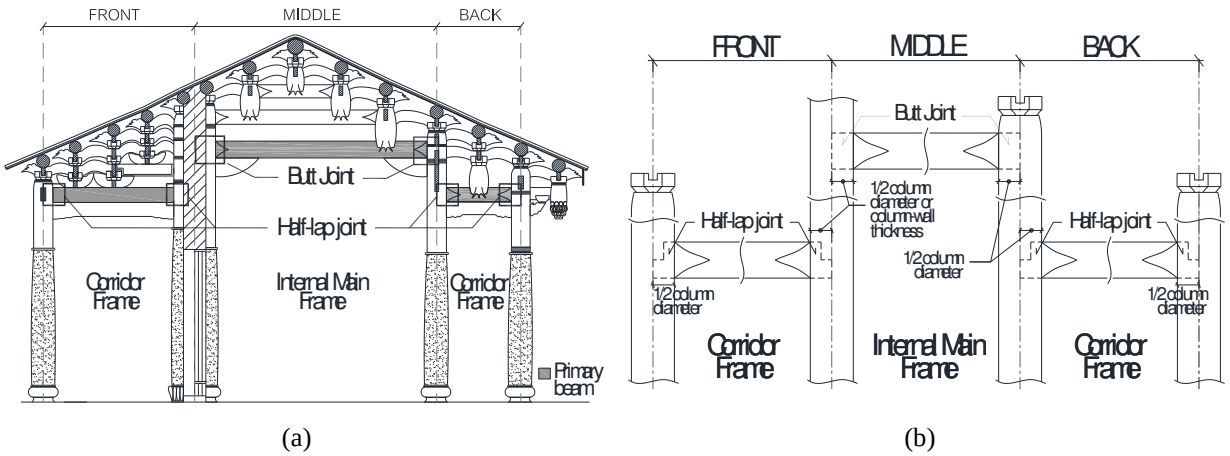

(a) (b)

Figure 5. Typical Dieh-Dou timber frame showing (a) the areas where the structural resistance column-beam system and (b) its close-up of the joint designs commonly used.

Assuming that the basic moment-resistance mechanism of the mortise-tenon joints depends largely on the penetration depth of the primary beam tenon and, friction force that was resulted from the partial embedment of timber when loaded perpendicular to the grain, the above assumptions led to the following questions:

1. Does different joint design and penetration depth have any effect of the structural performance of primary beam-column connection when subjected to lateral force?
2. Will the performance of a half-penetrating butt-jointed beam be comparatively weaker than the half-penetrating lap-jointed beam and full-penetrating butt-jointed beam?

To address the first two questions above, butt joint and lap joints were used to simulate three different scenarios of primary beam-column connections, namely half-penetrating butt joint case for Specimen 1, full- and half-penetrating butt joint case for Specimen 2 and half-penetrating lap-joint case for Specimen 3.

As the assembly method for structural members of the three specimens is generally the same, Specimen 1 was used an example to illustrate the assembly method of the main frame specimen (Figure 6). Dowel connections were commonly used between the vertical members, such as the column and Dou members, Gua-Tong and Dou members, and Gua-Tong and beam members. The rest of the horizontal members (beam and Shu members) were basically connected with their adjacent members by either slotting into the mortises of the vertical posts (column and Gua-Tong) or simply stacked within the rectangular-cut notch of the Dou members.

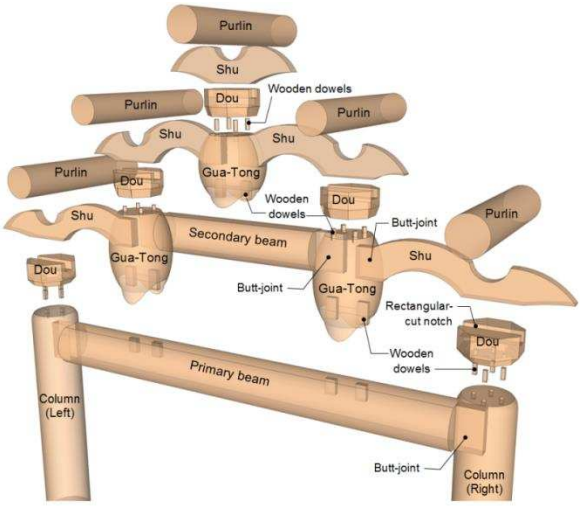

Figure 6. General assembly method for the structural members of the test specimens

2.1.3. Choice of wood material

Two types of wood materials (China Fir and Taiwan Red Cypress) were used to study the effects of different types of wood material on the structural behaviour of the primary beam-column connections. Specimen 1 and Specimen 3 were fabricated entirely using China Fir (Cunninghamia lanceolate) whilst Specimen 2 was assembled by a mixture of Taiwan Red cypress (Chamaecyparis formosensis) and China Fir. The wood material of the Specimen 2 was originally Taiwan Red cypress, which was once part of prototype specimen as mentioned above. For certain structural members that were already missing or damaged, replicas were made using China Fir. An overview of the types of wood material used, primary beam-column joint designs and key dimensions of the three specimens is summarized in Figure 7.

Table 1. Estimation of roof loads for the specimens

2.2. Experiment program

A total of three full-scale specimens were tested to study the in-plane structural behaviour of the Dieh-Dou internal main frame. The building width interval of the Dieh-Dou timber frame has been studied [1] and can be broadly sorted into three main categories: 3, 4.5 and 6 m. Base on Shih's [32] roof dead load calculation, the estimated roof weights for 3-, 4.5- and 6-m building width intervals were 20, 31 and 40 kN, respectively (Table 1).

Pitch angle (degree)	Unit Load (kN/m^2)	Length (m)	Building width (m)	Area (m^2)	Estimated Roof Load (kN)
23	4.4	1.54	3	4.63	20.4 → 20
		1.54	4.5	6.94	30.5 → 31
		1.54	6	9.26	41.0 → 40

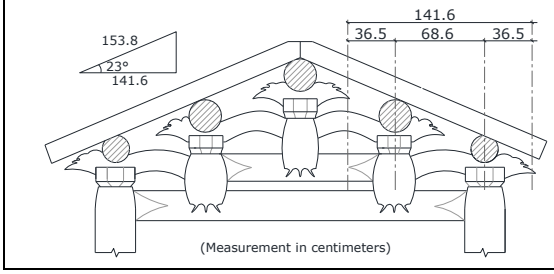

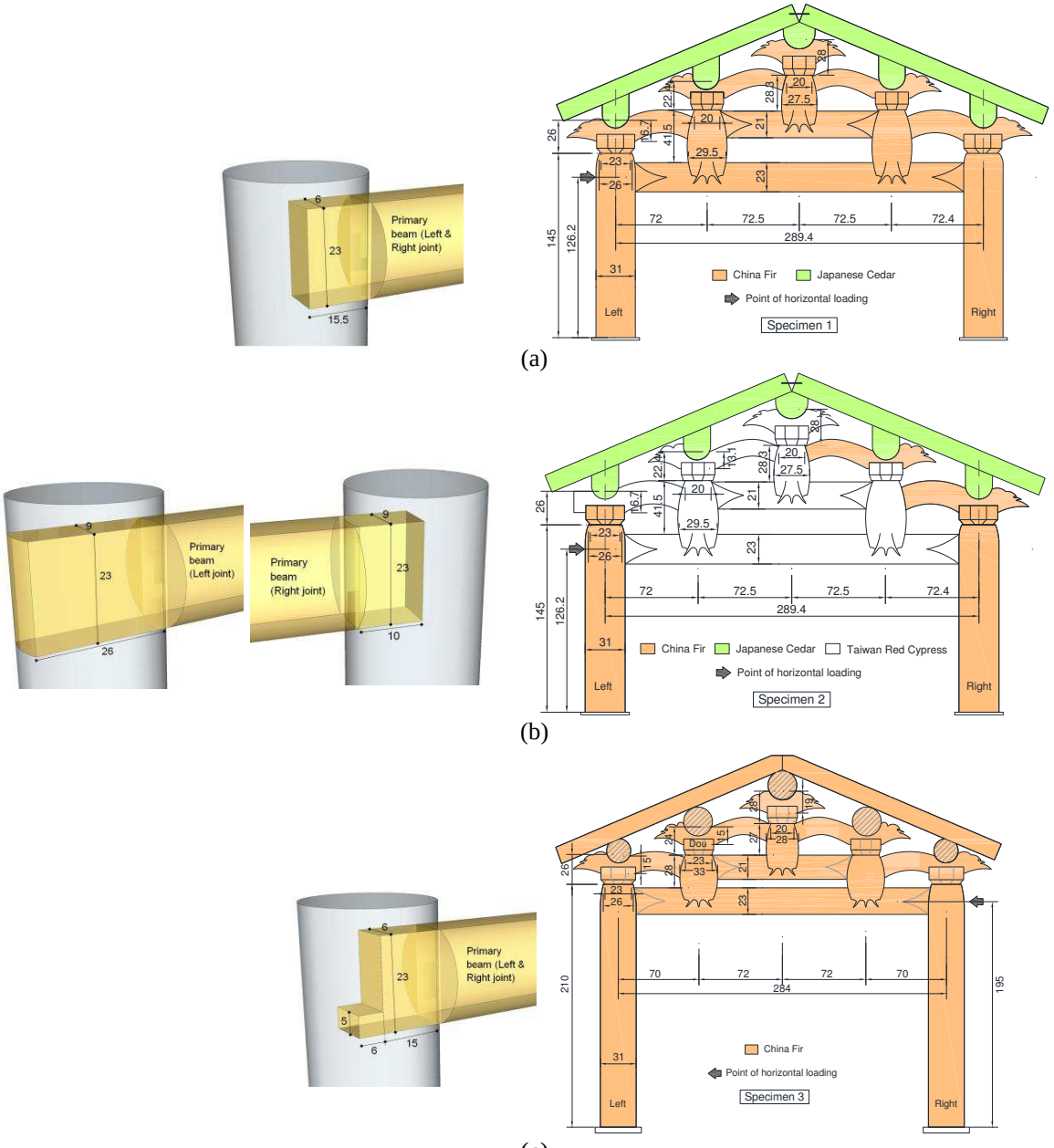

Figure 7. Types of wood material used and key dimensions for the three specimens (Measurements in centimeters)

All three specimens were fabricated and/or repaired by Master carpenters in Taiwan. As part of an international collaboration project, Specimen 1 and 2 were tested in Kyoto University, Japan; whilst Specimen 3 was tested in National Cheng Kung University, Taiwan. Except for the difference in primary beam-column joint design (Figure 9) and wood material used, Specimen 1 is basically a replica of Specimen 2. In the case Specimen 3, all structural members were fabricated closely base on the geometric dimensions of the prototype specimen (Figure 3a). The main differences between Specimen 1 and 3 include the joint design of primary beam-column and column height (due to the difference in test frame setup at two regions). From the roof load estimation in Table 1, the vertical load for building width intervals of 3 to 6m range between 20 and 40kN. Hence, the lower and upper limits of estimated vertical loads were selected for the tests, where 20kN vertical load was used for Specimen 1 and 2 and 40kN was applied on Specimen 3. The experiment setup and testing procedures carried out at two regions will be explained.

The experiment setup for Specimen 1 and 2 is shown in Figure 8. Under different combinations of vertical and horizontal loads, cyclic loading test was applied at a displacement speed of 0.05 mm/sec by a hydraulic actuator of 250kN capacity. Vertical load is simulated by employing the downward pulling force concept via the pulley-wire system. Two pairs of vertical rods, located at the front and back of the specimen was first bolt-secured with a C-channel steel that was fixed at the top of timber rafters. The vertical rods were then connected to two pairs of pulley-wire loading systems. To generate a vertical loading of 20kN, a pair of hydraulic actuators at the lower end of the reaction frame (each having a 100kN capacity) was used simultaneously to power the two pairs of pulley-wire loading systems, by creating a constant backward pulling force throughout the test. The horizontal loading protocol began at 1/100 rad, and gradually increased from 1/50, 1/30, 1/25 and finally reaching a maximum of 1/12 rad displacement target. One cycle test was conducted for each displacement target. A total of 51 channels of data were collected from the test, of which 10 channels were used as system monitors and the remaining 41 channels were assigned as displacement transducers.

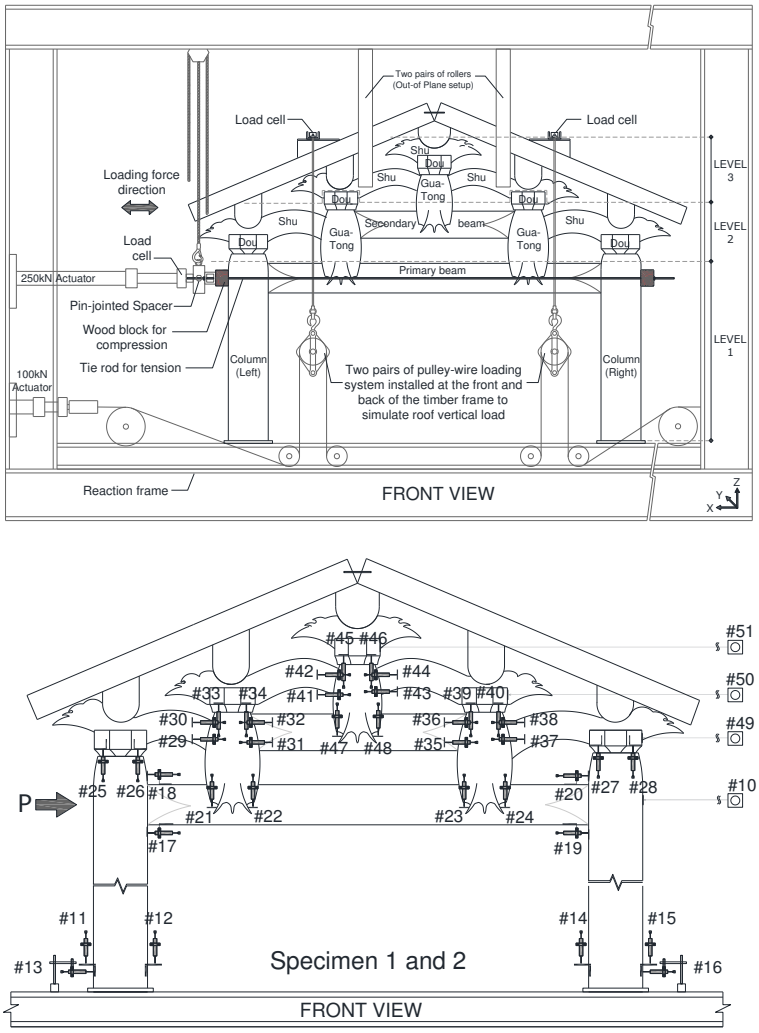

Figure 8. Overview of experiment setup for Specimen 1 and 2

The experiment setup of Specimen 3 differs from the above mainly due to the absence of pulley-wire system and a complete reaction frame, as shown in Figure 9. To simulate vertical load, specially-made steel block setup were used instead. The initial plan was to hang the steel blocks directly on top of each purlin position. However, having considered of potential instability that might occur during installation and testing process, two additional rafters were added on top of the specimen to fix the purlins in position and also to provide a more stable fixation surface for the steel block setup. Unlike the conventional western type of rafter design, with minimum section dimension (W x H) of 50 x 100 mm, which basically functions as the primary load-bearing elements of the roof truss, the function of 'oriental-type' rafter

played a supportive role instead, hence the section dimension of the Dieh-Dou type rafter (minimum (W x H): ~39 x 18 mm) was much thinner. To address the stability issue of the steel block installation, section dimensions of the two rafters were increased to 120 x 120 mm. Special steel frames with rollers installed internally were designed to prevent the specimen from out-of-plane collapse (Figure 9).

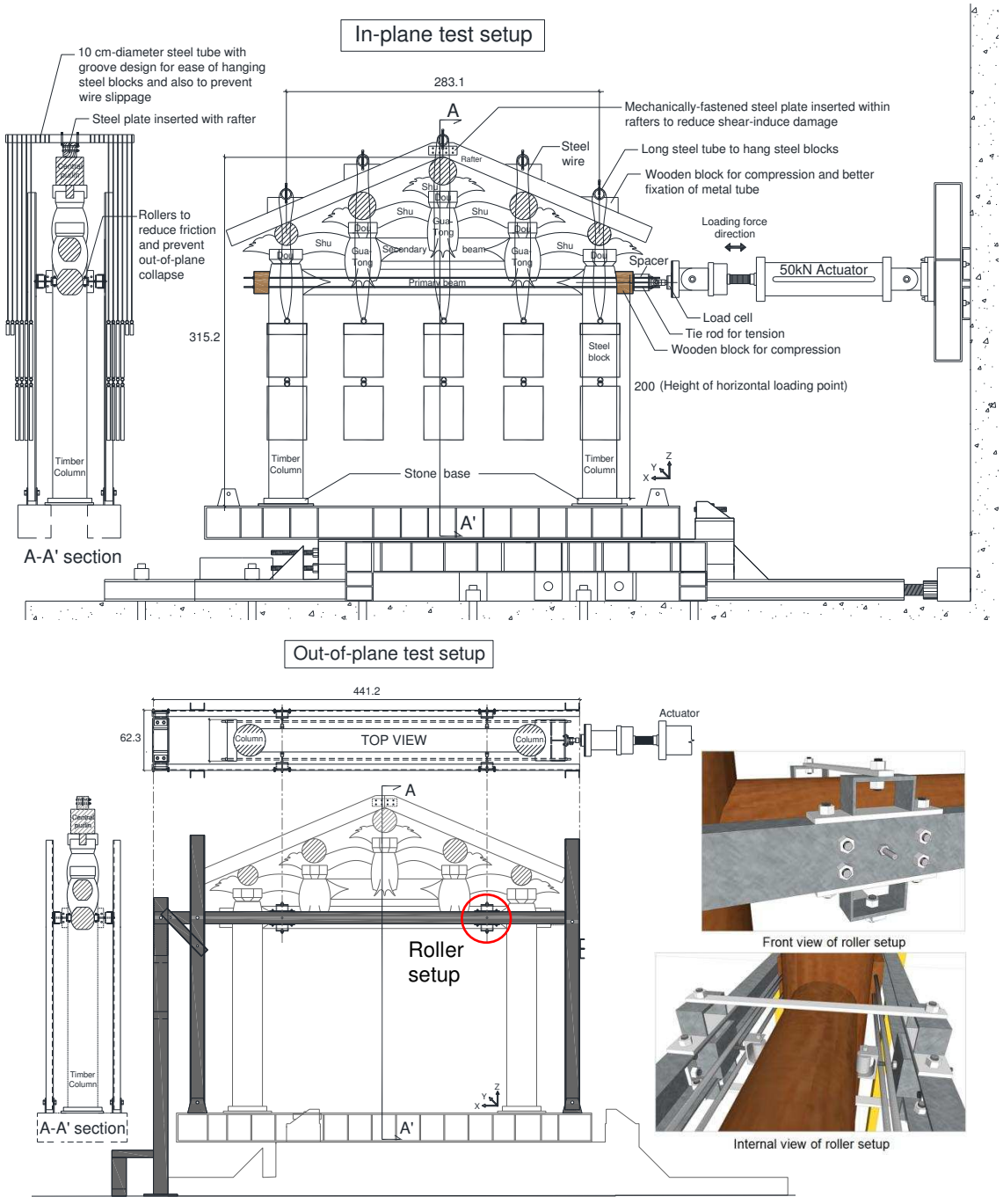

Figure 9. Test setup for Specimen 3 (Measurements in centimeters)

Similarly, the specimen was subjected to large displacement test with vertical loading of 40kN. Cyclic horizontal loading was applied at a displacement speed of 2 mm/sec by a hydraulic actuator of 50kN capacity. The loading protocol began from displacement target of 1/100, 1/50, 1/30, 1/25, 1/15 and finally reaching a maximum of 1/12 radian. A total of 49 channels of data were collected from the test, of which 40 channels were assigned for displacement transducers, 4 channels for strain gages and the remaining 5 channels were used as system monitors (Figure 10). Digital cameras were used throughout all three tests to record the global behaviour of the specimens. The main parameters for the tests are vertical loads and rotation.

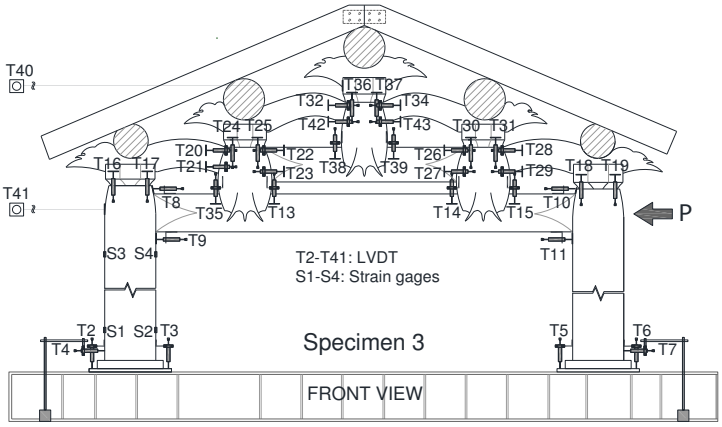

Figure 10. Positioning of the measuring devices for Specimen 3

3. THEORETICAL MODEL

3.1. Model hypotheses

From the global perspective, a single Dieh-Dou main frame is composed of several layers of bracket complexes, joined together by horizontal members (Shu and secondary beam) and short post members (Gua-Tong), which eventually sit on top of the primary beam supported by two columns. Apart from the two columns and three Gua-Tong members that were loaded parallel to the grain, the rest of the members were generally loaded perpendicular to the grain. For the sake of easy reference and further discussion, the main frame is divided horizontally around the beam intersecting regions into three levels, as shown in Figure 11.

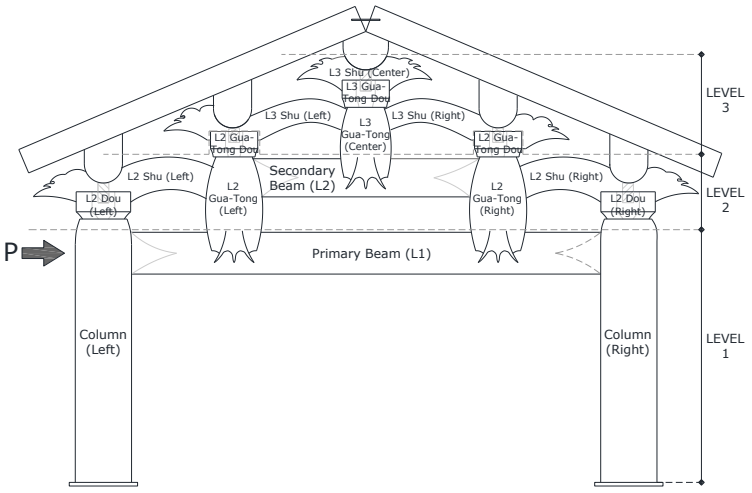

Figure 11. Naming of structural members and level designation for the Dieh-Dou internal main frame

Assuming the Dieh-Dou main frame behaved like a portal frame, column restoring force and the primary beam-column connection played the primary role in moment-resisting mechanism while the complex brackets above the primary beam played a secondary role. Hence, Ban's [17] approach on estimating the column restoring force and other vertical post members will be applied in this study. Since all structural members deformed mainly along the loading force direction and return in-place when no loading force was exerted, thus rotational spring is proposed to estimate the behaviour of the structural members. A mechanical model based on the following assumptions was composed:

1. Considering the Dou members and Gua-Tong members as short post-like members and the Shu members as horizontal tie members, when the post-like members and its adjoined tie members are subjected to the same embedment stress during the course of loading, the height of the bearing block spring, h, is thus assumed to be the combined height of the bearing block complex (Figure 12).
2. The depth of the 'bearing block spring', d, was considered by taking the average of the upper and lower contact depth values that the Dou member is adjoined with (Figure 12).
3. The rotational angle along the X-Z plane was only considered (Figure 8, 9 and 12). Any deformations that occurred along the X-Y plane were not considered in this study.
4. Friction is not considered at joint penetrating members (beam-column joint, Dou-Shu joint and Guo-Tong- Shu joint).
5. Deformation of global system was assumed to be the sum of each rotational deformation caused at each complex bracket and timber interlocking joint.
6. The proposed model is able to predict the initial stiffness, yielding point and secondary stiffness of each spring, with the exception of predicting the global system's ultimate strength.
7. With reference to Inayama's assumption [19,20], secondary stiffness of each spring was assumed as 1/8 of the initial stiffness.

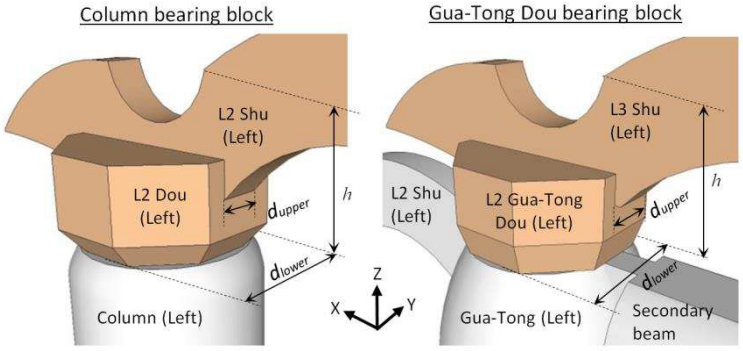

$$d = \frac{d_{lower} + d_{upper}}{2}$$

Figure 12. Explanatory for the definition of d and h in the estimation of rotational spring for different types of bearing block complexes

3.2. Global model for a single frame

By summing up all the contributions from the above sections and without considering the effects of rocking, the global load-deformation equation for a single frame (M_{Single}) can be generally expressed as

$$M_{Single} = M_C + M_{GT} + M_{BC} + M_{BG2} + M_{BG3} + M_{Bm1} + M_{Bm2} + M_H \quad (1)$$

where,

M_C : Contribution from column restoring force;

M_{GT}: Total contribution from the three Gua-Tong members at Level 2 and Level 3;

M_{BC}: Total contribution between the column bearing blocks at two ends;

M_{BG2}: Total contribution from the two Gua-Tong Dou members at Level 2;

M_{BG3}: Contribution from the Gua-Tong Dou member at Level 3;

M_{Bm1}: Contribution from the column-primary beam joint at two ends;

M_{Bm2}: Contribution from the Gua-Tong-secondary beam joint at two ends;

M_H: Total contribution from all the horizontal tie members (Shu members)

Similar to the mechanical modelling of the corridor structure as described by Yeo [16], the rotational spring represents the rotational behaviours of the bearing block members and all the joint-penetrating members. Using spring stiffness assumption proposed by Fujita [21-23], the column Dou and Gua-Tong complexes at level 2 and 3 are viewed as vertical-load bearing block members (Figure 18). Thus, they can be considered as five individual sets of single-tier serial springs ($R_{BC(L)}$, $R_{BC(R)}$, ${}_{L}R_{BG2}$, ${}_{R}R_{BG2}$ and R_{BG3}). As for the case of the 12 rotational springs that are found on both connection ends of each horizontal tie member, they can be considered as six pairs of parallel springs ($R_{Bm1(L)}$, $R_{Bm1(R)}$, $R_{Bm2(L)}$, $R_{Bm2(R)}$, ${}_{L}R_{S2(L)}$, ${}_{L}R_{S2(R)}$, ${}_{R}R_{S2(L)}$, ${}_{R}R_{S2(R)}$, ${}_{L}R_{S3(L)}$, ${}_{L}R_{S3(R)}$, ${}_{R}R_{S3(L)}$ and ${}_{R}R_{S3(R)}$). The final mechanical model for the Dieh-Dou internal main frame is illustrated as Figure 13a. For simplicity sake, a schematic global spring model (Figure 13b) will be used for the rest of the discussion. Detailed explanation and derivation of rotational springs and the mechanical modelling for the internal main frame have been described in Yeo [1,16] and will not be repeated in this paper.

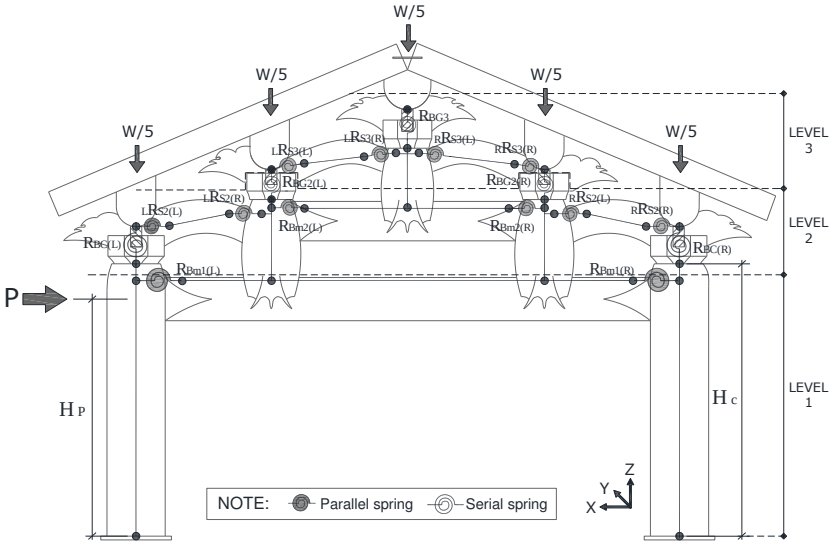

(a)

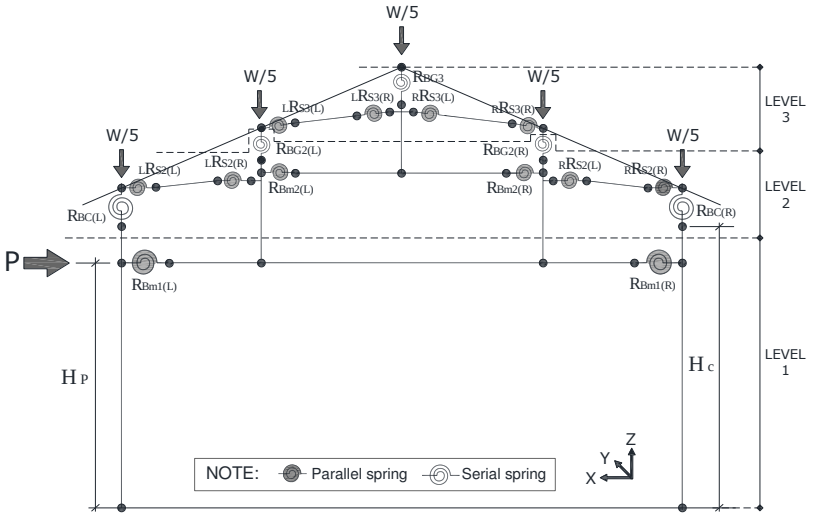

(b)

Figure 13. Proposed global model showing (a) the initial concept and (b) the final schematic global spring model

3.2.1 Contributions from vertical posts restoring force

Based on the practical design equations (Equation 2) provided by the Japanese Agency for Cultural Affairs [33] for the relationship between column restoring force and deflection, the calculation of the total restoring force contributed by the two columns and three Gua-Tong members is illustrated in Figure 14 and 15 and the equation below:

$$B_0 = (B_1 + B_2)/2, \quad P_0 = WB_0/H \quad \text{and} \quad (P/P_0)_{max} = 0.75 \tag{2}$$

Deflection ratio δ/B_0	0	0.025	0.05	0.1	0.15	1
Force ratio P/P_0	0	0.5	0.65	0.75	0.75	0

where,

B_0 : Average column width of vertical post top (B_1) and vertical post bottom or widest width (B_2) [mm]

P_0 : Estimated horizontal shear force [kN]

W : Axial force acting on each vertical post (column or Gua-Tong) [kN]

H : Height of vertical posts (column or Gua-Tong) [mm]

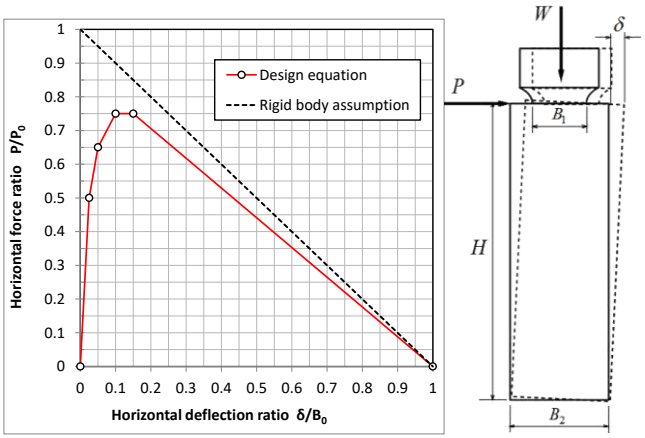

Figure 14. Normalized column restoring force–deflection relationship [34]

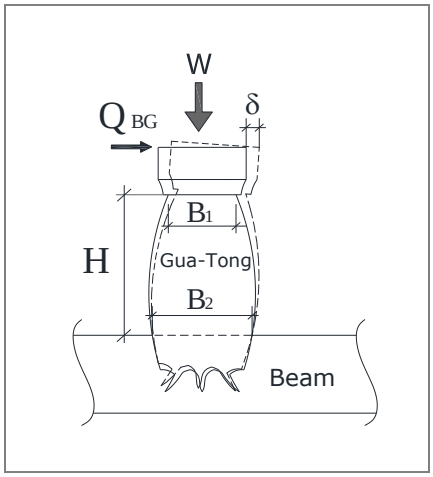

Figure 15. Definition of B_1 and B_2 parameters for Gua-Tong calculation

3.2.2 Contributions from the vertical post-beam joint members

In this section, the contributions from the column-primary beam joint and Gua-Tong-secondary beam joint are described. With reference to Figure 16, consider a situation where the relative rotational angle between the column and beam joint at both ends are assumed to be the same as the global shear deformation angle (θ_G) and that the shear force is in equilibrium with the moment resulted from the joint rotations between the primary beam and two columns. For simplicity, calculation is reduced to either right or left side of the beam-column joint and, subsequently multiplies the total effect by two. The following equilibrium relationship can be written as

Column-primary beam joint:

$$\left.\begin{aligned} Q_{Bm1} H_P &= 2M_{Bm1(L)} = 2R_{Bm1(L)} \cdot \theta \\ \theta &= u_P / H_P \end{aligned}\right\} \quad \Rightarrow Q_{Bm1} = \frac{2R_{Bm1(L)}}{H_P^{\,2}} \cdot u_P = K_{Bm1} \cdot u_P \tag{3}$$

Gua-Tong-secondary beam joint:

$$\left.\begin{aligned} Q_{Bm2} H_P &= 2M_{Bm2(L)} = 2R_{Bm2(L)} \cdot \theta \\ \theta &= u_P / H_P \end{aligned}\right\} \quad \Rightarrow Q_{Bm2} = \frac{2R_{Bm2(L)}}{H_P^{\,2}} \cdot u_P = K_{Bm2} \cdot u_P \tag{4}$$

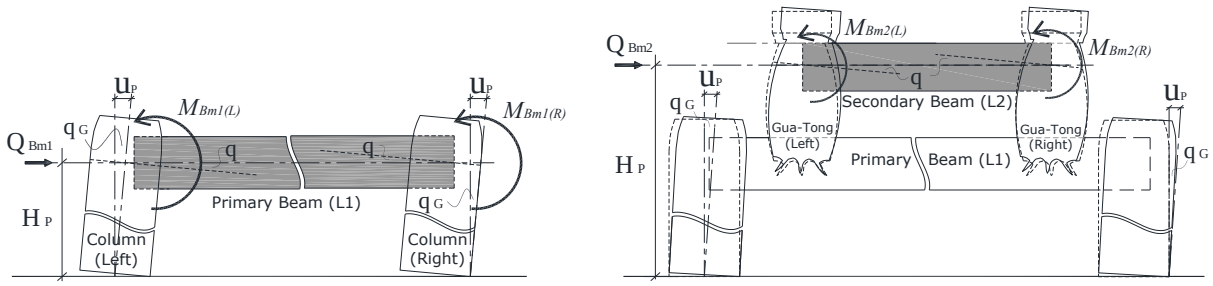

(a) (b)

Figure 16. Idealized scenarios of having the shear force in equilibrium with the moments resulted from: (a) two column–beam joints; and (b) Gua-Tong–secondary beam joints

3.2.3 Contributions from the bearing blocks at various positions

By simplifying the bearing block member, the embedment model for bearing block proposed by Kitamori et al. (2010) could be applied in the modelling. Generally, the relative rotational angles of the bearing blocks at various locations are assumed to be the same as the global shear deformation angle (θ_G). Considering the global structure is in equilibrium, under the balanced system of applied loads and reactions, the shear and moment diagrams for a single set of column bearing block and Gua-Tong-Dou complexes are illustrated in Figure 17. Without taking into consideration on the effects of vertical load, the equilibrium equation for the column bearing block at Level 2 and Gua-Tong-Dou complexes at level 2 and 3 are presented, respectively.

Column bearing block complexes:

$$\left.\begin{array}{c} Q_{BC} H_P = 2M_{BC(L)} = 2R_{BC(L)} \cdot \theta \\ \theta = u_P / H_P \end{array}\right\} \quad \Rightarrow Q_{BC} = \frac{2R_{BC(L)}}{H_P^{\,2}} \cdot u_P = K_{BC} \cdot u_P \tag{5}$$

Level 2 Gua-Tong Dou complexes:

$$\left.\begin{array}{c} Q_{BG2} H_P = 2M_{BG2(L)} = 2R_{BG2(L)} \cdot \theta \\ \theta = u_P / H_P \end{array}\right\} \Rightarrow Q_{BG2} = \frac{2R_{BG2(L)}}{H_P^{\,2}} \cdot u_P = K_{BG2} \cdot u_P \tag{6}$$

Level 3 Gua-Tong Dou complex:

$$\left.\begin{array}{c} Q_{BG3} H_P = M_{BG3} = R_{BG3} \cdot \theta \\ \theta = u_P / H_P \end{array}\right\} \quad \Rightarrow Q_{BG3} = \frac{R_{BG3}}{H_P^{\,2}} \cdot u_P = K_{BG3} \cdot u_P \tag{7}$$

where,

$$\theta_G = \frac{u_P}{H_P};$$

$$K_{BC} = 2R_{BC(L)} \cdot \frac{1}{H_P^2}; \quad K_{BG2} = 2R_{BG2(L)} \cdot \frac{1}{H_P^2}; \quad K_{BG3} = R_{BG3} \cdot \frac{1}{H_P^2}$$

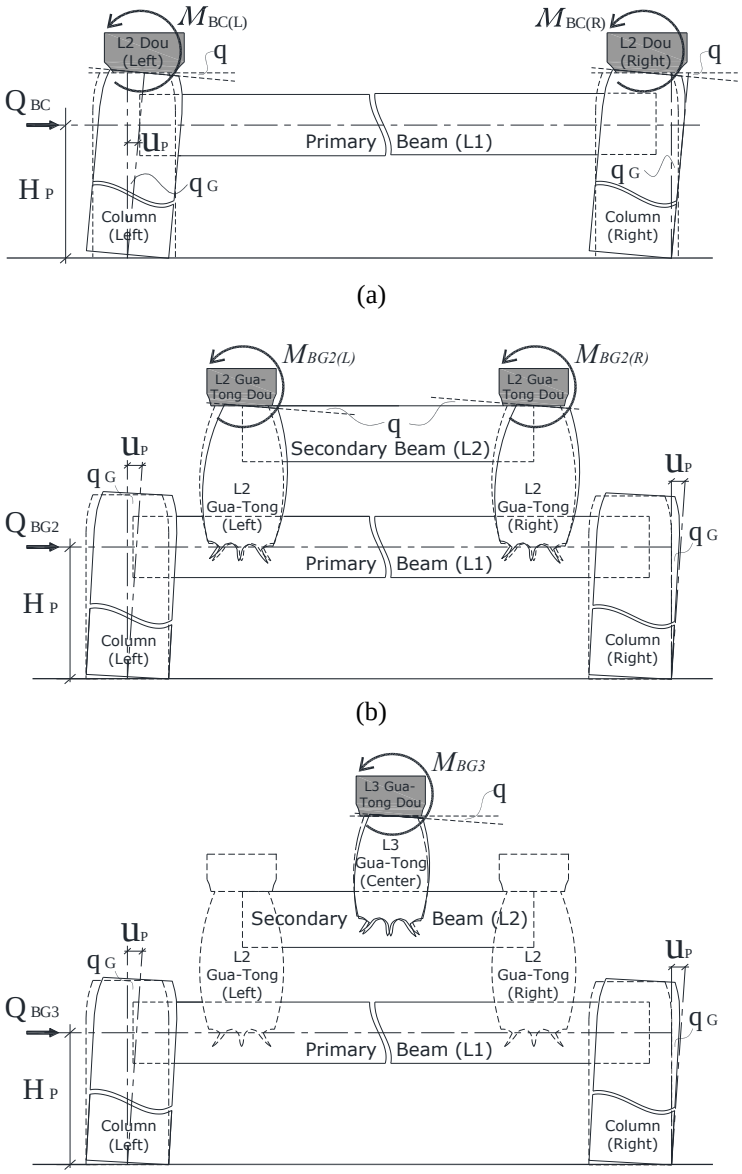

Figure 17**.** Assumed shear force is in equilibrium with the moments resulted from (a) two-column bearing blocks; (b) level 2 Gua-Tong-Dou bearing blocks; and (c) level 3 Gua-Tong-Dou bearing blocks

3.2.4 Contributions from rest of the horizontal tie members

Figure 18 presents a model for the contributions from the butt-jointed members (Shu and secondary beam) at level 2 and 3. The relative rotational angle between the butt-jointed horizontal tie members (Shu members) and the Gua-Tong complexes is assumed to be the same as the global shear deformation angle (θ_G). Consider the global structure is in equilibrium and that an additional lateral force (Q_H) is simultaneously acting on the eight butt joints that are holding the level 2 and 3 complex brackets of the left and right sections together.

Since the structural members from level 2 onwards are basically symmetrically arranged, hence similar to the column-primary beam approach in section 3.2.3, calculation method will be reduced to either the left or right side of the horizontal members and subsequently, multiply the total effect by two. In this study, rotational springs of the horizontal members from the left half (${}_LR_{S2(L)}, {}_LR_{S2(R)}, {}_LR_{S3(L)}, {}_LR_{S3(R)}$) side of the main frame will be chosen to work out the equilibrium equations.

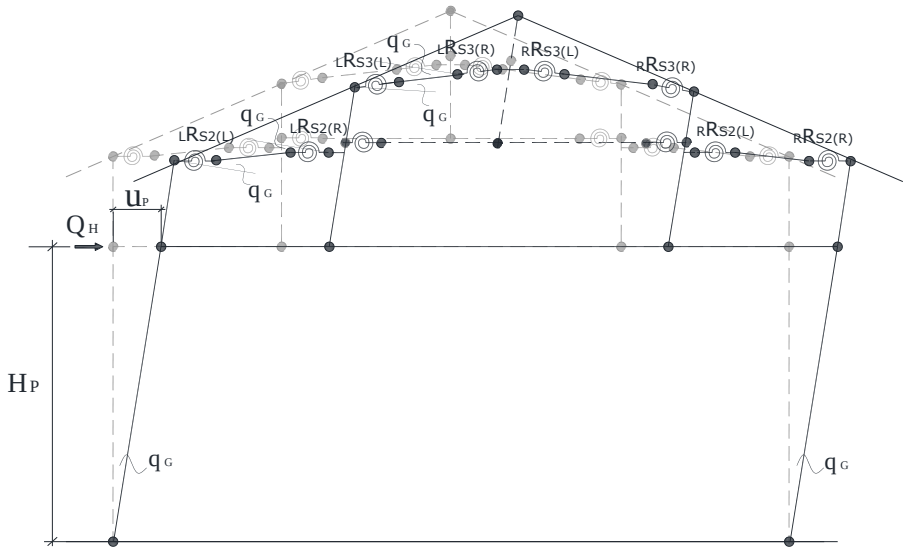

Figure 18**.** Contributions of butt joints of the Shu members when subjected to horizontal force

Assuming moment resistance occurred at these joints so as to counter the additional shear force, the summation of each joint moment will lead to the following relationship:

$$\begin{aligned} Q_H H_P &= 2\cdot\left({}_L M_{S2(L)} + {}_L M_{S2(R)} + {}_L M_{S3(L)} + {}_L M_{S3(R)}\right) \\ &= 2\cdot\left[\left({}_L R_{S2(L)} + {}_L R_{S2(R)} + {}_L R_{S3(L)} + {}_L R_{S3(R)}\right)\cdot\theta_G\right] \\ &= 2\cdot\left({}_L K_H\right)\left(\frac{u_P}{H_P}\right) \\ \Rightarrow Q_H &= K_H\cdot u_P \end{aligned} \tag{8}$$

where,

$$\theta_G = \frac{u_P}{H_P}; \qquad K_H = \frac{2\left({}_L R_{S2(L)} + {}_L R_{S2(R)} + {}_L R_{S3(L)} + {}_L R_{S3(R)}\right)}{H_P{}^2} = \frac{2\cdot {}_L K_H}{H_P^2}$$

3.2.5 Summation of all contributions for the global system

By summing up all the contributions from above sections and without considering the effects of rocking, the global load-deformation equation for a single Dieh-Dou internal main frame can be written as the following expression:

$$\begin{aligned} P &= Q_{Vertical\_Posts} + Q_{Bearing\_Blocks} + Q_{Beams} + Q_{Horizontal\_Ties} \\ &= Q_{VP} + Q_{BB} + Q_{Bm} + Q_H \\ &= K_{VP}\cdot u_P + K_{BB}\cdot u_P + K_{Bm}\cdot u_P + K_H\cdot u_P \\ &= \left[K_{VP} + K_{BB} + K_{Bm} + K_H\right]\cdot u_P \end{aligned} \tag{9}$$

where,

$K_{VP} = \left(WB_{0\_C} + WB_{0\_GT2} + WB_{0\_GT3}\right)\cdot\frac{1}{H_P}$ ➢ Column & 3 Gua-Tong restoring force

$$K_{BB} = \left(2R_{BC(L)} + 2R_{BG2(L)} + R_{BG3}\right) \cdot \frac{1}{H_P^2}$$ ➢ Level 2 & 3: Bearing block complexes

$$K_{Bm} = \left(2R_{Bm1(L)} \cdot 2R_{Bm2(L)}\right) \cdot \frac{1}{H_P^2}$$ ➢ Level 1 & 2: Beam-connections

$$K_H = \frac{2 \cdot {}_L K_H}{H_P^2} = \frac{2\left({}_L R_{S2(L)} + {}_L R_{S2(R)} + {}_L R_{S3(L)} + {}_L R_{S3(R)}\right)}{H_P{}^2}$$ ➢ Level 2 & 3 Horizontal tie members

4. RESULTS AND DISCUSSION

4.1. Estimation of material constant

Due to limited resources, there was not enough wood material to conduct material test quantitatively for Specimens 1 to 3. One truncated China Fir wood material from one of the columns of two Specimens was retrieved from Kyoto University after the 2010 test. However, the column material was generally not in good condition; hence only certain parts of the truncated column were used to conduct material test. As most the embedment (except for columns and Gua-Tong) observed in the test specimens were loaded perpendicular to the grain (Figure 21), four radial-direction samples were used to carry out partial compression test. An average E_{90} value of 0.054 kN/mm^2 was obtained, as shown in Table 2. In the case of Taiwan red cypress and China Fir that was used in Specimen 2 and 3, respectively, no extra wood material was made available for material test; hence the E_0 values for the above two wood species were quoted from the guidelines provided by the CPAMI [35]. As the conditions of the specimens were slightly damp during testing period, decision was made to use the recommended adjustment factor of 1/50 provided by AIJ [36]. By multiplying the quoted E_0 values with an adjustment factor of 1/50, the final E_{90} values for Taiwan red cypress (Specimen 2) and China Fir (Specimen 3) were 0.177 kN/mm^2 and 0.137 kN/mm^2, respectively (Table 2).

Table 2. Overview of the E_{90} values for Specimen 1, 2 and 3

Specimen	Wood material used	E_0 (kgf/cm^2)	E_0 (kN/mm^2)	E_{90} (kN/mm^2)	Reference source
1	China Fir	--	--	0.054	From partial compression tests
2	Taiwan red cypress	90,000	8.829	0.177	CPAMI [35]; AIJ [36]
	China Fir	--	--	0.054	Same as Specimen 1
3	China Fir	70,000	6.867	0.137	CPAMI [35]; AIJ [36]

4.2. Global frame deformation

From on-site test observations (Figure 19) and measured values (Figure 20), column rocking generally led to the lateral displacement the entire structure. First sign of visible deformation started at the primary beam-column region, with column rocking and beam-column joint rotation dominating the entire testing cycles. Visible rotational deformation of the column bearing block complex (i.e. Column Dou and Level 2 Shu member) generally began from 1/30 rad test onwards. By comparing the rotational behaviours of the column, primary beam, Gua-Tong members, Dou members and the global frame of all three Specimens (Figure 20), significant rotational values were mainly observed on the column, column Dou and primary beam members. The above observations follow well with the results of Suzuki & Maeno [25] where it was observed that column restoring force played a major role towards the total restoring force when the frame deformation is small (less than ±1/50), and the bending moments from tie beams will take over major role when deformation increases.

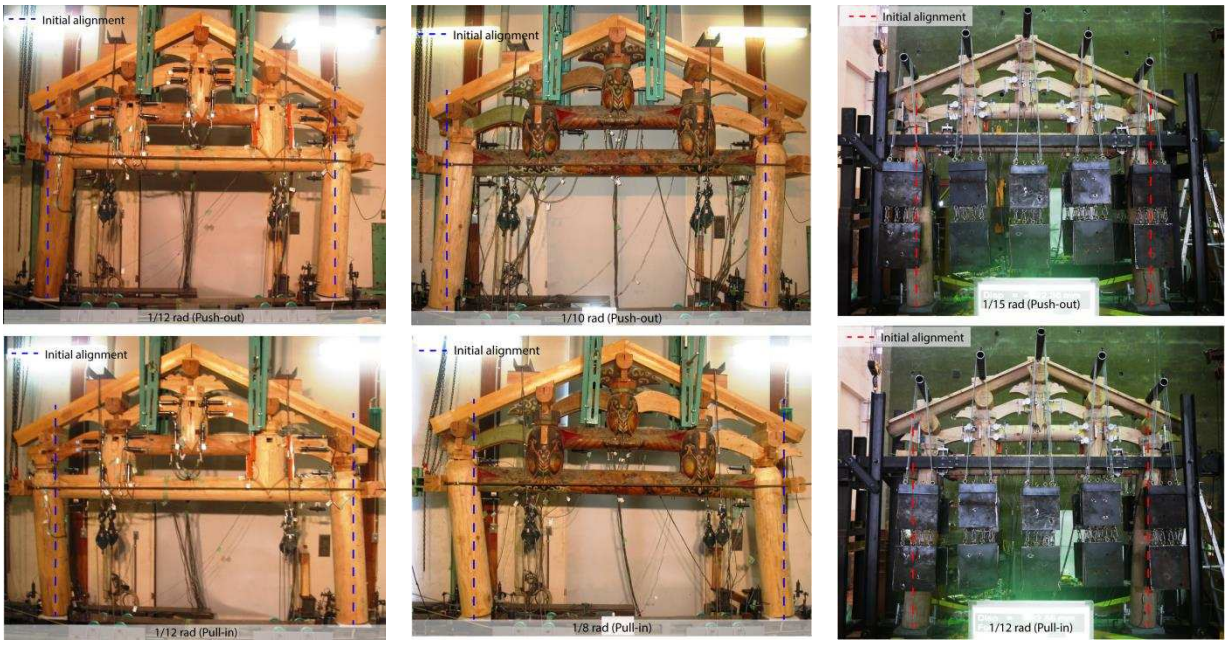

(a) (b) (c)

Figure 19. Typical global frame deformation observed on the three specimens during large displacement tests: (a) Specimen 1; (b) Specimen 2 and; (c) Specimen 3.

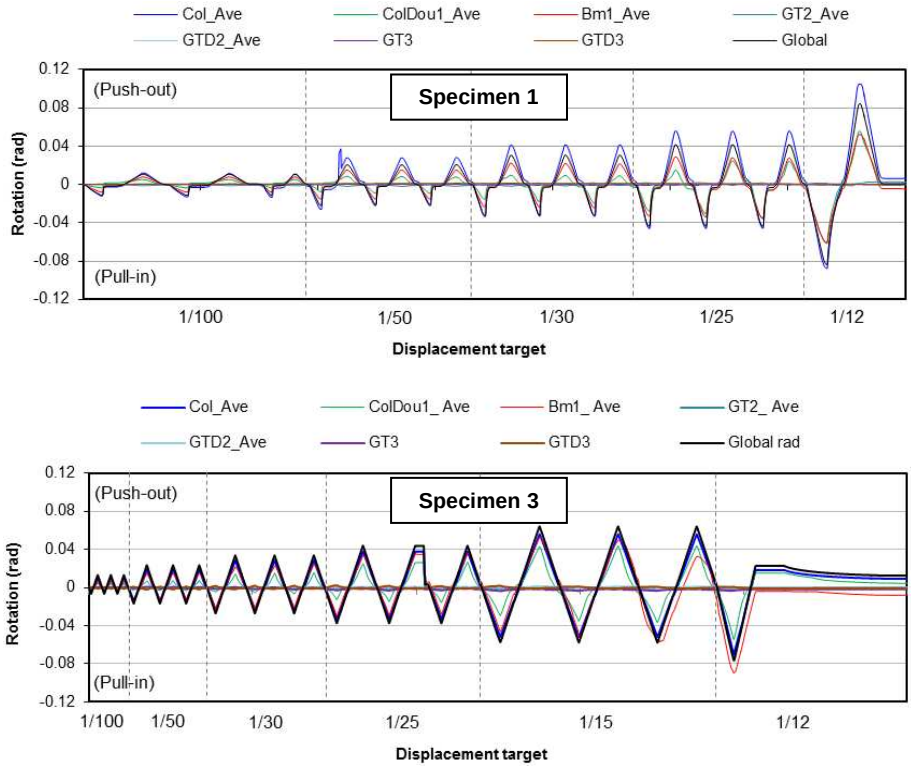

Note:

Global	: Rotation of global frame	GT2_ Ave	: Average rotation of two Gua-Tong at Level 2;
Col_Ave	: Average rotation of two columns;	GTD2_Ave	: Average rotation of two Gua-Tong Dou at Level 2;
ColDou1_Ave	: Average rotation of two column Dou;	GT3	: Rotation of Gua-Tong at Level 3;
Bm1_Ave	: Average of primary beam's two joint rotations	GTD3	: Rotation of Gua-Tong Dou at Level 3;

Figure 20. Overview of the rotational behaviours of column, primary beam, Gua-Tong members, Dou members and the global frame between Specimen 1 and 3

Evidence of slight rotation (ranges between ±0.01rad) was recorded for the Gua-Tong, Gua-Tong Dou and rest of the members from level 2 onwards. As the rotation was too small to be detected by the naked eye, the structural members from the secondary beam level onwards could be generally assumed as rigid. Since the test observations are in good agreement with the model hypotheses in section 3.1, it is highly probable that the global structure tends to behave like a portal frame.

4.3. Damage patterns of structural members

As more visible damages were observed in Specimen 2 and 3; hence photographic records of the main damage regions of Specimen 2 and 3 are presented (Figure 21). Three critical areas, namely the primary beam-column regions, the column Dou and column connection regions and, the Dou and Shu member connection regions, were commonly observed in all three specimens. Typical damage patterns include column rocking (Figure 19), vertical shearing (induced by beam rotation) around the column mortise (Figure 21a), joint rotation around the column-column Dou region (Figure 21b), and mortise damage around the Dou-Shu connections (Figure 21c).

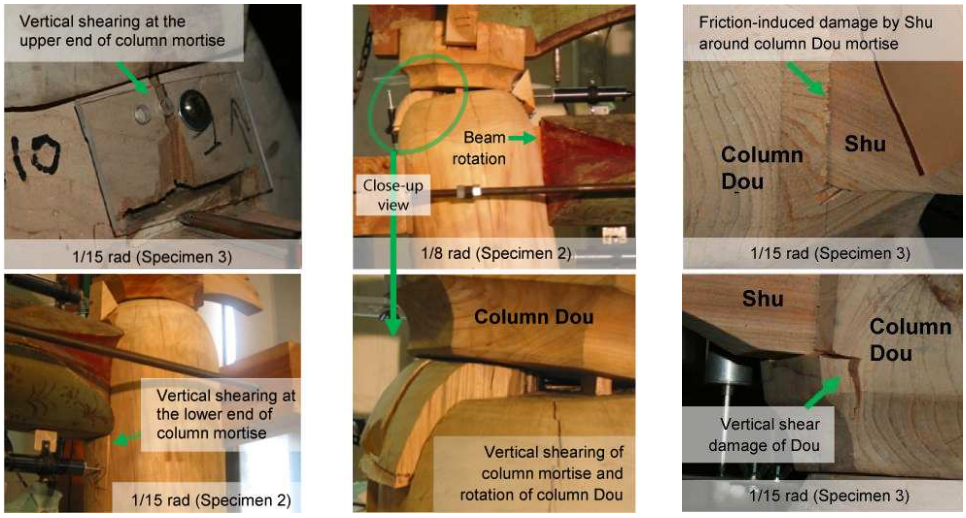

(a) (b) (c)

Figure 21. Typical damage patterns observed: (a) vertical shearing around upper and lower ends of column mortise; (b) joint rotation around column and column Dou region; (c) mortise damage around Dou-Shu connections

The penetration depth of the beam tenon has direct effect on the vertical shearing of column mortise. As shown in Figure 22, when joint A has tenon length more than or equal to the diameter of the column, more damage was observed around the column mortise region when subjected to greater horizontal force (Figure 23). This is especially seen in the case of Specimen 2 where the 'longer' tenon at joint A began to damage the upper region of column mortise from 1/30 rad and caused maximum damage at 1/8 rad (Figure 21b). In the case of joint B in Specimen 1 and Specimen 2 (Figure 23), damage to the column mortise was less severe comparatively as the tenon length was only half of the column's diameter. Assuming that the primary beams of both specimen 1 and 2 were subjected to the same rotational angle, a longer tenon (full-penetrating type) tends to have greater surface contact with the surrounding column mortise region than a shorter tenon (half-penetrating type). There will be a higher tendency for the longer beam tenon to counter more moment-resistance and embedment within the column mortise than the shorter tenon (Figure 23).

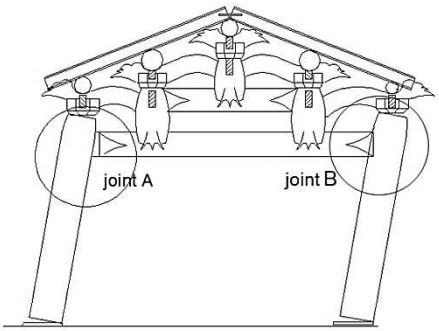

Figure 22. Different joint type designs for primary beam of Specimen 2 [14]

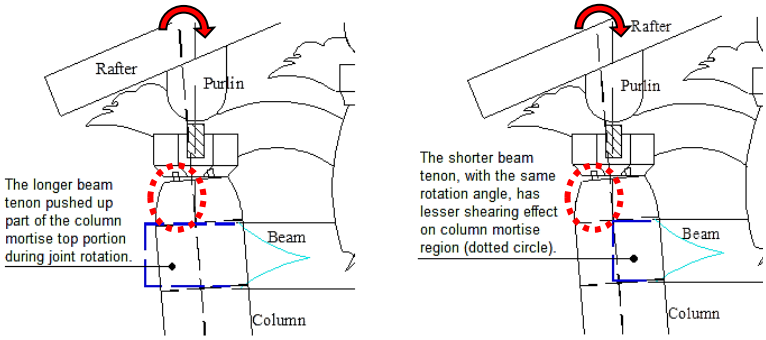

Figure 23. Difference in beam tenon depth on the shearing effect of column mortise region [14]

4.4. Effect of primary beam joint design on the initial stiffness of global frame

An overview of the hysteretic loops of the three specimens' force-deflection curves are presented in Figure 24 and the various key values measured from the hysteresis loops of the three specimens are summarised in Table 3. The initial stiffness values of the Pull-in ($K1^+$) and Pull-out tests ($K1^-$) were estimated by dividing the P_{max} value with the δ_{max} value measured from their respective loop. As shown in Figure 24, severe pinching is commonly observed in the hysteretic loops of all three specimens. This suggests that permanent deformation (e.g. partial embedment) occurred on the structural members at early stage. A point to note is the dipping trend observed during the 1/10 rad Push-out displacement test of Specimen 2. This was mainly due to the rotation of the full-penetrating beam joint with the left column mortise that led to the first visible sign of vertical shearing on the left column mortise top portion, subsequently causing a sudden jerk of the transducer during time of recording.

Although the hysteretic loops of the Dieh-Dou timber frames showed poorer energy dissipation capacity compared to the idealized elastic system, and that the initial stiffness K1 (Table 3) generally decreases as the displacement increases, the ability of the entire timber frame to sustain large deformability and continued to maximise its global shear-resistance proved that the highly ductility nature of Dieh-Dou timber frames, even in times of large deformation.

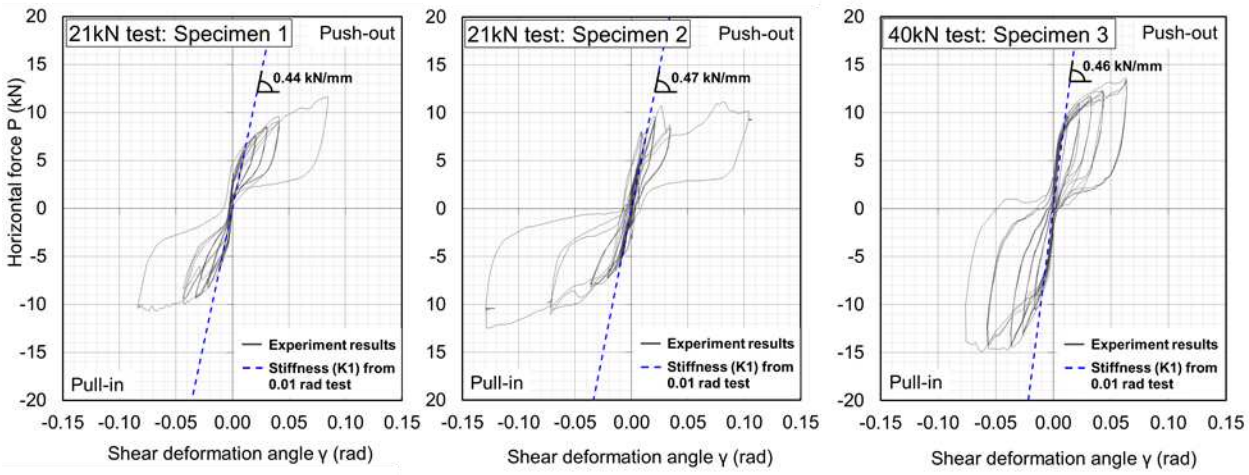

(a) (b) (c)

Figure 24. Overview of the force-deflection curves of the three specimens

Table 3. Large displacement test results for the three specimens

	W (kN)	γ_{max} (rad)	Cycle	$\delta_{max,cycle}$ (mm)	δ_{max_AVE} (mm)	$P_{max,cycle}$ (kN)	P_{max_AVE} (kN)	$K1_{max,cycle}$ (kN/mm)	$K1_{max\_AVE}$ (kN/mm)	Dissipated energy (J)	Dissipated energy (Ave) (J)	H_{eq} (%)	H_{eq} (Ave) (%)
Specimen 1	21	1/100	1	13.75	13.78	5.70	5.99	0.42	0.44	56.0	57.7	7.3	6.6
			2	13.78		6.09		0.44		58.5		6.6	
			3	13.80		6.19		0.45		58.5		6.0	
		1/50	1	26.70	26.68	7.74	7.86	0.29	0.29	154.4	147.1	9.6	8.1
			2	26.65		7.92		0.30		144.4		7.4	
			3	26.68		7.91		0.30		142.4		7.2	
		1/30	1	39.45	39.68	8.77	8.72	0.22	0.22	254.5	243.6	10.8	9.3
			2	39.70		8.57		0.22		239.1		9.0	
			3	39.90		8.81		0.22		237.2		8.2	
		1/25	1	52.35	53.13	9.76	9.16	0.19	0.17	361.4	330.6	11.9	9.9
			2	53.50		8.54		0.16		326.4		10.1	
			3	53.35		9.17		0.17		303.8		7.6	
		1/12	1	101.48	101.48	11.02	11.02	0.11	0.11	839.5	839.5	16.5	16.5
Specimen 2	21	1/100	1	13.82	13.73	6.39	6.41	0.46	0.47	52.47	52.01	6.1	6.1
			2	13.82		6.41		0.46		52.72		6.0	
			3	13.55		6.42		0.47		50.83		6.2	
		1/50	1	26.48	26.46	8.41	8.29	0.32	0.31	145.76	136.80	9.0	7.9
			2	26.43		8.26		0.31		134.94		7.8	
			3	26.48		8.20		0.31		129.69		7.0	
		1/25	1	40.70	42.93	8.20	8.22	0.20	0.19	257.99	253.49	14.0	11.3
			2	43.95		8.28		0.18		253.35		10.0	
			3	44.15		8.17		0.19		249.14		9.7	
		1/15	1	89.70	89.70	10.81	10.81	0.12	0.12	685.92	685.92	14.6	14.6
		1/10	½	131.15	131.15	10.22	10.22	0.08	0.08	1037.14	1037.14	15.6	15.6
		1/8	½	162.75	162.75	11.99	11.99	0.07	0.07	1477.56	1477.56	19.6	19.6
Specimen 3	40	1/100	1	18.54	18.52	8.42	8.46	0.45	0.46	99.56	98.07	7.14	6.75
			2	18.52		8.47		0.46		97.87		6.63	
			3	18.49		8.48		0.46		96.79		6.48	
		1/50	1	38.97	38.84	10.01	10.51	0.26	0.27	306.54	302.08	13.79	12.58
			2	38.84		10.78		0.28		309.10		12.88	
			3	38.71		10.73		0.28		290.61		11.06	
		1/30	1	59.24	59.15	12.30	12.31	0.21	0.21	544.56	525.76	14.91	13.31
			2	59.18		12.25		0.21		524.87		13.13	
			3	59.04		12.38		0.21		507.84		11.88	
		1/25	1	73.27	77.46	13.35	13.28	0.18	0.17	712.08	734.22	17.66	15.55
			2	79.33		13.22		0.17		742.34		14.83	
			3	79.77		13.28		0.17		748.24		14.15	
		1/15	1	112.21	117.27	14.13	13.91	0.13	0.12	1246.65	1235.84	21.19	19.23
			2	119.87		13.85		0.12		1230.01		18.09	
			3	119.75		13.76		0.12		1230.88		18.41	
		1/12	½	155.82	155.82	13.85	13.85	0.09	0.09	1641.41	1641.41	23.37	23.37

NOTE:

W	Constant vertical load;
P^{+}_{max}	Maximum push-out force;
P^{-}_{max}	Maximum pull-in force;
P_{max_AVE}	Maximum average force;
δ^{+}_{max}	Maximum push-out displacement;
δ^{-}_{max}	Maximum pull-in displacement;
δ_{max_AVE}	Maximum average displacement;
$K1^{+}_{max}$	Initial stiffness measured along push-out direction;
$K1^{-}_{max}$	Initial stiffness measured along push-out direction;
$K1_{max\_AVE}$	Average initial stiffness;
H_{eq}	Damping ratio (%)

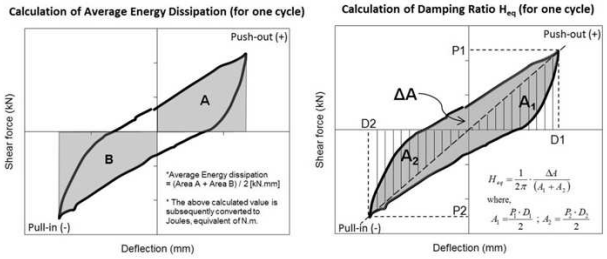

From the measured data of Table 3, energy dissipation between Specimen 1 and 3 showed a positive correlation with the vertical loads. In other words, when the vertical load roughly doubled from 21kN (Specimen 1) to 40kN (Specimen 3), the amount of energy dissipated from the global frame of Specimen 3 is also twice as much. However, the maximum initial stiffness ($K1_{max}$) values and maximum shear force (P_{max}) presented alternative views. The $K1_{max}$ values of Specimen 1 and 3 were found to be relatively similar between the displacement tests of 1/100 rad and 1/25 rad. The anticipated lower P_{max} values for Specimen 3 were also not observed. Instead, the average global P_{max} values of Specimen 3 were generally higher than Specimen 1 by around 3kN. Hence, theoretical column restoring force contribution of Specimen 3 when subjected to 40kN of vertical load was calculated, using the force-deflection relationship (Equation 10) for column restoring force [17].

$$\frac{PH}{WB} = 1 \Rightarrow P = \frac{WB}{H} \tag{10}$$

where, P = horizontal live load (Restoring force for 1 column); W = constant vertical load; B = column width; H = column height.

$$\therefore \; P_{Sp.3\_2columns} = \left(\frac{20 \times 0.285}{1.95}\right) \times 2 \approx \underline{\underline{5.99 \text{ kN}}}.$$

By subtracting the calculated column restoring force value of 5.99kN with 8.66kN (1/100 rad test result in Table 2), an estimated value of 2.47kN for the combined joint resistance occurring at various parts of the frame. Assuming that most of the joint resistance arises from the primary beam-column lap-joint, the 'lap-joint effect' might have possibly helped to increase the overall joint resistance by roughly 2 kN. The lap-joint effect became more prominent as displacement increases from 1/100 to 1/30 rad. Beyond 1/30 rad, the upper region of column mortise started to yield in the form of vertical shear failure (Figure 15). Similar trend is also observed for the initial stiffness (K1) values for Specimen 1 and 3 in Table 2. From the above results, the lap-joint effect might have compensated for the lower P_{max} values via a 'stiffer' beam joint, subsequently helped to reinstate the initial stiffness of the global frame similar to that of Specimen 1. Apart from increasing the vertical load to improve the global stability of the frame, the addition of a lap-joint at critical moment-resisting regions might help to enhance the overall frame stability further.

4.5. Verification of theoretical models

Figure 25 presents the predicted models with relation to their respective test results. The upper graphs illustrate the force-deformation relationship of the three specimens when subjected to the Push-out tests. Base on the above models from the Push-out tests, the results are then reflected inversely to generate the models for the Pull-in tests, as shown by the lower graphs of Figure 25.

From the upper graphs, contributions from column (blue solid line), primary beam (red solid line) and column bearing block (brown dash line) dominated the outcome of the global behaviour (black solid line) of the model. Minimal effects were observed for the remaining structural elements, where each element in all three specimens generally contributed around 1 kN of shear resistance for displacement target of up to ±0.06 rad. The above predicted behaviours are in line with the test results where most of the observed deformations were around the jointing regions of the columns, primary beam and column bearing block complexes (Figure 19 to 21). In addition, the lowered shear resistance performance of Specimen 2's primary beam with respect to Specimen 1 also fits well with observed deformation where the effects of longer beam tenon (Figure 7b) and stronger material property (Table 2) of Specimen 2's primary beam joint led to the vertical shearing of the column mortise (Figure 21a and 21b), subsequently affecting the global structural performance.

The mechanical models for the three test results generally showed a relatively good fit between the experimental and predicted results (Figure 25). The above mechanical prediction is only valid for the estimation of the primary and secondary stiffness because each spring stiffness was assumed to behave up to bi-linear stage. Thus, the predicted models appear to increase infinitely. The predicted models can only consider the behaviour occurring along the loading force direction (X-Z plane); hence it is unable to predict the out-of-plane failure scenario and ultimate failure condition. In order to predict the ultimate stage precisely, detailed evaluation of the failure criterion of each member is required so that a more systematic numerical calculation method can be carried out to predict the global behaviour of the timber frame. Although a more conservative approach was adopted for this prediction, the mechanical models and assumptions are regarded as valid in general.

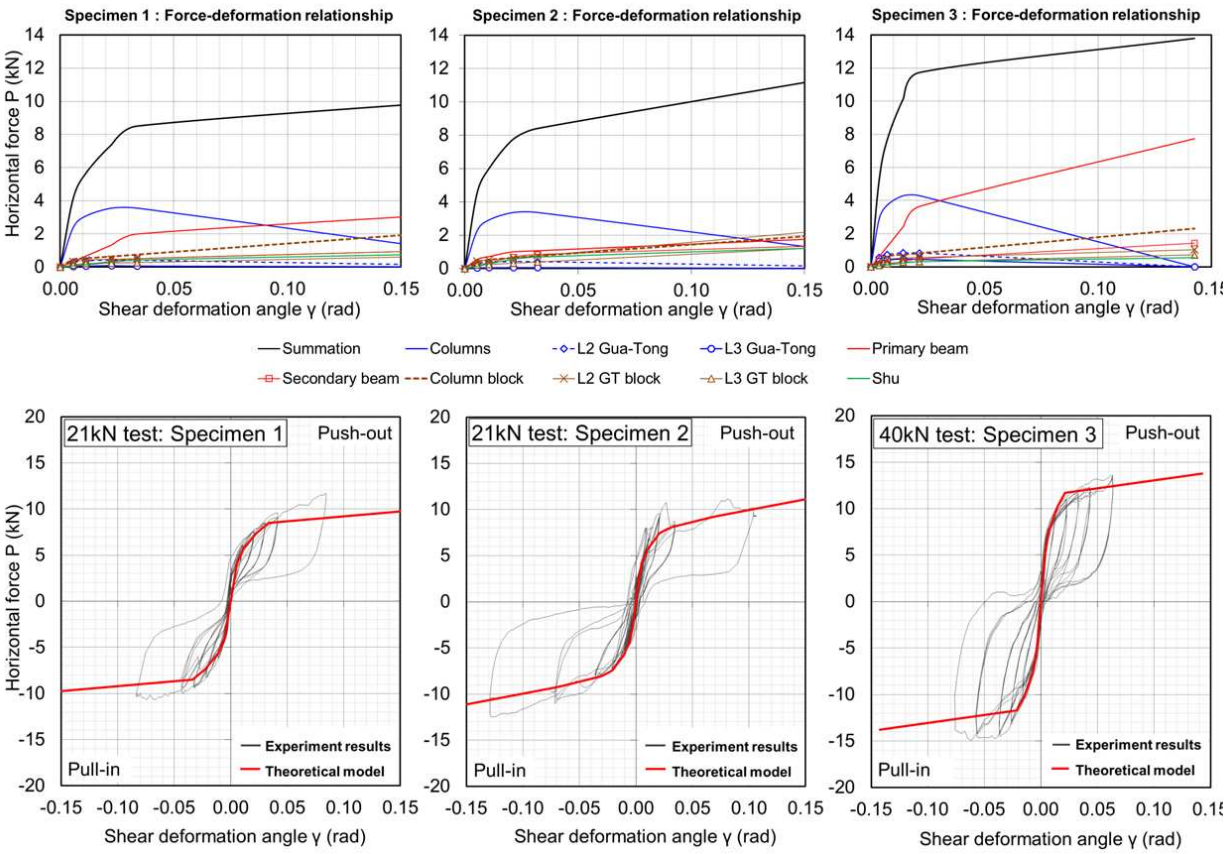

(a) (b) (c)

Figure 25. Comparison of the theoretical models of the internal main frames with static test results: (a) Specimen 1; (b) Specimen 2 and (c) Specimen 3

5. CONCLUSION

Three full-scale traditional Dieh-Dou timber frames were tested under cyclic horizontal loading with constant vertical loading to compare their structural behaviour. The following conclusions can be drawn based upon the experimental results:

1. Column rocking tends to dominate the global frame displacement. Visible deformation of the internal main frame generally began from 1/30 rad onwards. Typical deformation patterns include joint rotation around primary beam-column and column Dou-column regions, vertical shear around the upper and lower end of column mortise, embedment around primary beam-column regions and vertical shearing around the mortise regions of the Dou members.
2. The upper structure generally remained rigid despite column rocking; hence the global structure could be considered as a portal frame, where column restoring force and the primary beam-column connection undertake the primary moment-resisting mechanism while the complex bracket structures above the primary beam play a secondary role.
3. Column restoring force contributed mainly to the frame's shear resistance when displacement is small. When frame deformation is more than 1/50 rad, bending moment from the primary beam dominated the frame's global restoring force.
4. Although vertical load has significant effect on the horizontal strength and stiffness of the entire structure, the addition of lap-joint or other similar joints at critical load-bearing joint areas, such as the primary beam-column region, might help to improve the overall stability of the Dieh-Dou timber frame structure.
5. Longer beam tenon increases the probability of column mortise shearing. The use of mechanically stronger wood for beam member might also increase the chances of column mortise shearing further. Hence, the choice of wood material for moment-resistance members such as primary beam and column should be taken into consideration.

6. By assuming each rotational spring behaves in a bi-linear manner, the theoretical model can only estimate the in-plane primary and secondary spring stiffness; the out-of-plane failure phenomena and ultimate failure load cannot be predicted using this current model. Although the predictions tend to be on the conservative side, the mechanical models generally fit well with the experiment results; thus, the assumptions made in this study are valid in general.

ACKNOWLEDGMENTS

The tests for Specimen 1 and 2 were performed at the Laboratory of Structural Function (LSF), RISH, Kyoto University in Japan while Specimen 3 was conducted at the Department of Architecture, NCKU in Taiwan. Special thanks go to all members of both institutions for making all the tests possible. Sincere gratitude is also extended to the Tan Kah Kee Foundation (Singapore) for awarding the Tan Ean Kiam Postgraduate Scholarship to the first author.

FUNDING

The static test for Specimen 3 was fully supported by the Taiwan Ministry of Science and Technology (previously known as 'National Science Council') under the grant project number NSC-101-2221-E-006-258-.

REFERENCES

[1] Yeo S Y. Structural performance of Taiwanese traditional Dieh-Dou timber frame [PhD dissertation]. Taiwan, Tainan: National Cheng Kung University. 2016.
[2] Architecture and Building Research Insitute (ABRI). A preliminary report on the structural failures of buildings: 921 Chi-chi earthquake [in Chinese]. Taipei: Ministry of Interior; 1999.
[3] Council for Cultural Affairs (CCA). Post-earthquake reconnaissance report for historic buildings: 921 Chi-chi earthquake and 1022 Chiayi earthquake [in Chinese]. Taipei: CCA; 2000.
[4] CCA. Post-earthquake structural evaluation report for historic buildings: 921 Chi-chi earthquake and 1022 Chiayi earthquake (Volume 1 and 2) [in Chinese]. Taipei: CCA; 2000.
[5] Hsu M-H, Kuo H-Y. & Tseng Y-J. The evaluation of the timber global frame structural characteristics [Chapter 5]. In: A study on the earthquake-induced damage of historic buildings and its future maintenance: (1) Timber and Bamboo structures [in Chinese]. Edited by NCKURDF. Taipei, Taiwan: CCA; 2001.
[6] NCKU Research and Development Foundation (NCKURDF). A study on the earthquake-induced damage of historic buildings and its future maintenance: (1) Timber and Bamboo structures [in Chinese]. Taipei, Taiwan: Executive Yuan Council for Cultural Affairs (CCA); 2001. Research report No. CCA89-16.
[7] Tsai P-H. Seismic evaluation of traditional timber structures in Taiwan [PhD dissertation]. UK, Bath: University of Bath. 2009.
[8] King WS, Yen JY, Yen YN. Joint characteristics of traditional Chinese wooden frames. Engineering structures 1996; 18(8): 635-644.
[9] Chang W-S, Hsu M-F, Komatsu K. Rotational performance of traditional Nuki joints with gap I: theory and verification. J Wood Sci 2006; 52(1):58-62.
[10] Chang W-S, Hsu M-F, Komatsu K. Rotational performance of traditional Nuki joints with gap II: the behavior of butted Nuki joint and its comparison with continuous Nuki joint. J Wood Sci 2007; 53(5): 401-407.
[11] Hwang, S-J, Lin M-L, Tsai M-J. 2007. The performance of timber mortise-tenon joint in Taiwan traditional buildings. Research report no. NCREE-07-28. Taipei, Taiwan: National Centre for Research on Earthquake Engineering (NCREE) [in Chinese].
[12] D'Ayala, D, Tsai P-H. Seismic vulnerability of historic Dieh-Dou timber structures in Taiwan. Engineering structures 2008; 30(8): 2101-2113.
[13] Hsu M-F, Chang W-S. The study of Taiwanese Traditional Dieh-Dou timber frame bracket complex structural behavior [in Chinese]. Taipei, Taiwan: National Science Council; 2010. Research report No. NSC 99-2221-E-006-156-.
[14] Yeo S Y, Chang W-S, Hsu M-F, Komatsu K. The structural behaviour of timber frame under various roof weights - using Taiwanese traditional Die-Dou timber frame as case study. In: EAAC Committee (ed.), Proceedings of the East Asian Architectural Culture International Conference (EAAC), 12-14 May 2011, Singapore. NUS: Singapore.
[15] Yeo S-Y, Hsu M-F, Komatsu K, Chung Y-L, Chang W-S . Shaking Table Test of the Taiwanese Traditional

Dieh-Dou Timber Frame. International Journal of Architectural Heritage 2016; 10(5): 539–557. DOI: 10.1080/15583058.2015.1009574
[16] Yeo S-Y, Komatsu K, Hsu M-F, Que Z. Mechanical model for complex brackets system of the Taiwanese traditional Dieh-Dou timber structures. Advances in Structural Engineering 2016; 19(1): 65-85. DOI: 10.1177/1369433215618269
[17] Ban S. Study of statics for structures of temple and shrines Part 1. In: Proceedings of technical papers of annual meeting of Architectural Institute of Japan (AIJ), 252-258, 1941 [in Japanese].
[18] Ban S. Study of statics for structures of temple and shrines Part 2. In: Proceedings of technical papers of annual meeting of AIJ, 259-268, 1941 [in Japanese].
[19] Inayama M. Embedment Theory of Timber and Its Application. Ph.D. thesis. The University of Tokyo; 1991 [in Japanese].
[20] Inayama M: Study on compression perpendicular to the grain in wood Part 4 Analytical functions for the relation between compression load and elastic deformation perpendicular to the grain in wood. In: Summaries of technical papers of annual meeting Architectural Institute of Japan, 907-908, September, 1993 [in Japanese].
[21] Fujita K, Kimura M, Ohashi Y, Sakamoto I. Shaking Table Test of 'Kumimono' used in Traditional Wooden Architecture Part 5 Static Lateral Loading Test of DEGUMI Bracket Complex. In: Summaries of technical papers of annual meeting Architectural Institute of Japan, 159-160, September, 1999 [in Japanese].
[22] Fujita K, Sakamoto I, Ohashi, Y, Kimura M. Static and dynamic loading tests of bracket complexes used in traditional timber structures in Japan. In: WCEE 2000, the 12th world conference on earthquake engineering. Auckland, New Zealand.
[23] Fujita K, Kimura M, Ohashi Y, Sakamoto I. Hysteresis Model and Stiffness Evaluation of Bracket Complexes used in Traditional Timber Structures Based on Static Lateral Loading Tests. J Struct Constr Eng, Architectural Institute of Japan (AIJ) 2001; 543: 121-127 [in Japanese].
[24] Suzuki Y, Katagihara K, Iwasa Y, Takata K, Yamamoto M, Goto M, Kitahara A. Dynamic characteristics and seismic performance of traditional wooden structure by shaking table tests. In: Proceedings of U.S.-Japan Joint Workshop and Third Grantees Meeting U.S. - Japan Cooperative Research in Urban Earthquake Disaster Mitigation 2001; 328-337. Seattle, USA.
[25] Suzuki Y, Maeno M. Structural mechanism of traditional wooden frames by dynamic and static tests. Structural Control and Health Monitoring 2006; 13(1): 508-522. DOI: 10.1002/stc.153
[26] Kitamori A, Jung K, Hassel I, Chang W-S, Komatsu K, Suzuki Y. Mechanical Analysis of Lateral Loading Behavior on Japanese Traditional Frame Structure Depending on The Vertical Load. In: WCTE 2010, World conference on timber engineering. Trentino, Italy.
[27] Fang D P, Iwasaki S, Yu M H, Shen Q P, Miyamoto Y, Hikosaka H. Ancient Chinese timber architecture, I: experimental study. Journal of structural engineering 2001; 127(11): 1348-1357. DOI:10.1061/(ASCE)0733-9445(2001)127:11(1348)
[28] Fang D P, Iwasaki S, Yu M H, Shen Q P, Miyamoto Y, Hikosaka H. Ancient Chinese Timber Architecture. II: Dynamic Characteristics. Journal of Structural Engineering 2001; 127(11), 1358–1364. DOI: 10.1061/(ASCE)0733-9445(2001)127:11(1358)
[29] Chun Q, Yue Z, Pan J W. Experimental study on seismic characteristics of typical mortise tenon joints of Chinese southern traditional timber frame buildings. Science China: Technological Sciences 2011; 54(9): 2404-2411. DOI: 10.1007/s11431-011-4448-3
[30] Yue Z. Traditional Chinese Wood Structure Joints with an Experiment Considering Regional Differences. International Journal of Architectural Heritage 2014; 8(2): 224–246. DOI: 10.1080/15583058.2012.688179
[31] Shiue, Chyn. 2006. Dismantling and investigation report for Hsinchu county historic building: Bei-Pu Jiang-Shi ancestral temple. Hsinchu, Taiwan: Hakka Affairs Council [in Chinese].
[32] Shih, C-H. 2014. Seismic evaluation of Ma-Dou Hu-Ji Temple [in Chinese]. In: Chao C-C (ed.), Emergency repair proposal for Tainan city historic building: Ma-Dou Hu-Ji Temple, Cultural Affairs Bureau. Tainan: Cultural Affairs Bureau, pp. 26-28 [in Chinese].
[33] Agency for cultural affairs. 2012. Implementation Guidance for Basic Seismic Assessment of Important Cultural Properties (Buildings), 2nd edn., Tokyo: Agency for Cultural Affairs.
[34] Komatsu, K. 2013, 'Lecture 4: Behavior & Modeling of Traditional Wooden Portal Frame Structures', lecture notes distributed in the topic Timber Structures and Functions (II), National Cheng Kung University (Taiwan), on 8 March 2013.
[35] Construction and Planning Agency for Ministry of Interior (CPAMI). 2011. Standard for the design and construction techniques of timber structures. 4th edn., CPAMI, Taipei [in Chinese].
[36] Architectural Institute of Japan (AIJ). Standard for structual design of timber structures. 4th ed. Tokyo: Maruzen; 2006 [in Japanese].